Photoproduction of bound states with hidden charm

Jia-Jun Wu and T.-S. H. Lee

Physics Division, Argonne National Laboratory, Argonne, Illinois 60439, USA

The photoproduction of the J/Ψ-^{3}He bound state ($[^3\text{He}]_{J/\Psi}$) on a ^{4}He target has been investigated using the impulse approximation. The calculations have been performed using several $\gamma + N \rightarrow J/\Psi + N$ models based on the Pomeron-exchange and accounting for the pion-exchange mechanism at low energies. The J/Ψ wave functions in $[^3\text{He}]_{J/\Psi}$ are generated from various J/Ψ-nucleus potentials which are constructed by either using a procedure based on the Pomeron-quark coupling mechanism or folding a J/Ψ-N potential ($v_{J/\Psi,N}$) into the nuclear densities. We consider $v_{J/\Psi,N}$ derived from the effective field theory approach, lattice QCD, and Pomeron-quark coupling mechanism. The upper bound of the predicted total cross sections is about 0.1–0.3 pb. We also consider the possibility of photoproduction of a six quark-J/Ψ bound state ($[q^6]_{J/\Psi}$) on the ^{3}He target. The compound bag model of NN scattering and the quark cluster model of nuclei are used to estimate the $[q^6]$-N wave function in ^{3}He by imposing the condition that the calculated ^{3}He charge form factor must be consistent with what is predicted by the conventional nuclear model. The upper bound of the predicted total cross sections of $\gamma + ^3\text{He} \rightarrow [q^6]_{J/\Psi} + N$ is about 2–4 pb, depending on the model of $\gamma + N \rightarrow J/\Psi + N$ used in the calculations. Our results call for the need of precise measurements of $\gamma + p \rightarrow J/\Psi + p$ and also the $\gamma + ^2\text{H} \rightarrow J/\Psi + n + p$ reactions near the threshold.

I. INTRODUCTION

The role of the gluon field in determining the interactions between nucleons and quark-antiquark ($Q\bar{Q}$) systems, which do not share the same *up* and *down* quarks with the nucleon, is one of the interesting subjects in understanding quantum chromodynamics (QCD). An important step toward this direction was taken by Peskin [1] who applied the methodology of the operator product expansion to evaluate the strength of the color field emitted by heavy $Q\bar{Q}$ systems. His results suggested [2] that the van der Waals force induced by the color field of J/Ψ on nucleons can generate an attractive short-range J/Ψ-N interaction. By using the effective field theory method, Luke, Manohar, and Savage [3] used the results from Peskin to predict the J/Ψ-nucleon forward scattering amplitude which was used to get an estimation that J/Ψ can have a few MeV/nucleon attraction in nuclear matter. Brodsky and Miller [4] further investigated the J/Ψ-N forward scattering amplitude of Ref. [3] to derive a J/Ψ-N potential ($v_{J/\Psi,N}$) which gives an J/Ψ-N scattering length of -0.24 fm. The result of Peskin was also used by Kaidalov and Volkovitsky [6], who differed from Ref. [4] in evaluating the gluon content in the nucleon, to give a much smaller scattering length of -0.05 fm. In a lattice QCD calculation, Kawanai and Saski [5] obtained an attractive J/Ψ-N potential $v_{J/\Psi,N} = -\alpha e^{-\mu r}/r$ with $\alpha = 0.1$ and $\mu = 0.6$ GeV, which gives a scattering length -0.09 fm. In Ref. [7], Brodsky, Schmidt, and de Teramond proposed an approach to calculate the potential between a $c\bar{c}$ meson and a nucleus by using the Pomeron-exchange model of Dannachie and Lanshoff [8]. The J/Ψ-N potential obtained in this approach is $v_{J/\Psi,N} = -\alpha e^{-\mu r}/r$ with $\alpha = 0.6$ and $\mu = 0.6$ GeV which gives a rather large scattering length -8.83 fm.

Our first objective in this paper is to explore whether these J/Ψ-N potentials, with rather different attractive strengths, can form J/Ψ-nucleus bound states. Following the well developed method in nuclear reaction theory [9], this is done by searching for bound states by solving the Schrödinger equation with a folding potential constructed by integrating the J/Ψ-N potential over the nuclear density. We will also consider the approach of Ref. [7] in predicting J/Ψ-nucleus bound states by the coherent sum of Pomeon-exchange between quarks in J/Ψ and all quarks in the nucleus. For each of the predicted bound $[^3\text{He}]_{J/\Psi}$ systems, we then estimate the photoproduction cross section of the $\gamma + ^4\text{He} \rightarrow [^3\text{He}]_{J/\Psi} + N$ reaction to facilitate future experimental investigations [10]. As discussed by Brodsky [11], the production of such bound states with hidden charms is feasible at JLab with 12 GeV upgrade because of the close proximity in rapidity of the heavy quark with the target spectators.

The second part of this work is motivated by the investigations by Brodsky and de Teramond [12] who found that the spin correlation of pp elastic scattering near the J/Ψ production threshold can be explained if one postulates the excitation of a hidden charm (c) state $|qqqqqqc\bar{c}\rangle$. Based on the similar consideration on the role of multiquark configurations, Brodsky, Chudakov, Hoyer, and Laget [13] suggested in a study of $\gamma + ^2\text{H} \rightarrow J/\Psi + n + p$ reaction that J/Ψ can interact strongly with the six-quark $[q^6]$ component of the deuteron wave function because the octet three-quark $[q^3]_8$ in the $[q^6]$ can directly interact with each quark in J/Ψ. These two works suggest the possibility that if J/Ψ overlap with a $[q^6]$ cluster in nuclei, a bound $[q^6]_{J/\Psi}$ system could be formed. It is of course very difficult, if not impossible, to estimate $[q^6]$-J/Ψ interaction. Instead, we will simply assume the existence of such states and use the previous works [14–21] on quark clusters in nuclei to explore how the cross sections of $\gamma + ^3\text{He} \rightarrow [q^6]_{J/\Psi} + N$ depend on the parameters characterizing the $[q^6]$-J/Ψ interaction within a potential model.

Our first task is to construct a model of $\gamma + N \rightarrow J/\Psi + N$ reaction. At high energies, it is well recognized that this
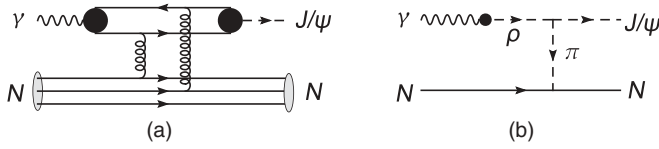
FIG. 1. Reaction mechanisms of $\gamma N \to J/\Psi + N$: (a) Pomeron-exchange, (b) pion-exchange.

reaction can be described by the Pomeron-exchange model with an interpretation [8,22–24] that Pomeron-exchange is due to the exchange of gluons within QCD. This is illustrated in Fig. 1(a). At low energies, one expects that mechanisms other than Pomeron-exchange could also contribute as can be seen in the exclusive ϕ photoproduction reaction on the nucleon [24–26]. However, very little investigation has been done for J/Ψ photoproduction in the near threshold region. As a first step, we will only consider the meson-exchange mechanism which can be calculated from using the partial decay width of $J/\Psi \to \pi\rho$ listed by the Particle Data Group [27] (PDG). With the vector meson dominance (VDM) assumption, this observed decay process indicates that J/Ψ photoproduction can also be due to the exchanges of a π meson with the nucleon, as illustrated Fig. 1(b).

We next consider the photonuclear reaction mechanism that a J/Ψ is produced from a nucleon in a nucleus with mass number A and then forms a bound state with the spectator B system which can be a $(A-1)$ nuclear system or a quark cluster $[q^{3(A-1)}]$ in the target nucleus A. With this commonly used impulse approximation, the reaction cross sections can be calculated from the $\gamma + N \to J/\Psi + N$ amplitude, which will be generated from the Pomeron-exchange and pion-exchange mechanisms described above, and the initial nucleon and final J/Ψ wave functions. The nucleon wave functions can be taken from the available nuclear models. The J/Ψ wave functions will be generated from various J/Ψ-B potentials mentioned above. For simplicity, we only present the predictions of the cross sections of $\gamma + [^4\text{He}] \to N + [^3\text{He}]_{J/\Psi}$ and $\gamma + [^3\text{He}] \to N + [q^6]_{J/\Psi}$ reactions.

In Sec. II, we present formula for calculating the $\gamma + N \to J/\Psi + N$ amplitudes from the Pomeron-exchange and pion-exchange mechanisms. The impulse approximation formula for calculating the cross sections of $\gamma + [A] \to [B]_{J/\Psi} + N$ are given in Sec. III. Our results are presented in Sec. IV. In Sec. V, we give a summary and discuss the necessary future work.

II. FORMULA FOR $\gamma + N \to J/\Psi + N$ REACTION

In the center-of-mass system, the differential cross section of $\gamma(\vec{q}) + N(-\vec{q}) \to J/\Psi(\vec{k}) + N(-\vec{k})$ with invariant mass W can be written

$$\frac{d\sigma}{d\Omega} = \left[\frac{(2\pi)^4 E_N(q)}{W}\right]\left[\frac{k E_{J/\Psi}(k) E_N(k)}{W}\right]$$
$$\times \frac{1}{4}\sum_{\lambda_\gamma,\lambda_{J/\Psi}}\sum_{m_s,m_s'}|\langle\vec{k}\lambda_{J/\Psi}m_s'|t(W)|\vec{q}\lambda_\gamma m_s\rangle|^2, \quad (1)$$

where $\lambda_{J/\Psi}$ and λ_γ are the helicities of the J/Ψ and photon, respectively, m_s is the z component of the nucleon spin, and $E_a(p) = [m_a^2 + \vec{p}^2]^{1/2}$ is the energy of a particle with mass m_a. The reaction amplitude is written as

$$\langle\vec{k}\lambda_{J/\Psi}m_s'|t(W)|\vec{q}\lambda_\gamma m_s\rangle$$
$$= \frac{1}{(2\pi)^3}\frac{1}{\sqrt{2E_{J/\Psi}(k)}}\sqrt{\frac{m_N}{E_N(k)}}\sqrt{\frac{m_N}{E_N(q)}}\frac{1}{\sqrt{2q}}$$
$$\times [\bar{u}_{m_s'}(p')\epsilon_\mu^*(k,\lambda_{J/\Psi})M^{\mu\nu}(p',p)\epsilon_\nu(q,\lambda_\gamma)u_{m_s}(p)], \quad (2)$$

where $u_{m_s}(p)$ is the nucleon spinor [with the normalization $\bar{u}_{m_s}(p)u_{m_s'}(p) = \delta_{m_s,m_s'}$], $\epsilon_\mu(k,\lambda_{J/\Psi})$ and $\epsilon_\nu(q,\lambda_\gamma)$ are the polarization vectors of J/Ψ and photon, respectively. Here we also have introduced the four-momenta for the initial and final nucleons:

$$p = (E_N(q), -\vec{q}); \quad p' = (E_N(k), -\vec{k}).$$

In the following subsections, we give formula for calculating the invariant amplitude $M^{\mu\nu}$ due to the Pomeron-exchange and meson-exchange mechanisms, as illustrated in Fig. 1.

A. Pomeron-exchange amplitude

Within the Pomeron-exchange model of Donnachie and Landshoff [8], the vector-meson photoproduction at high energies is due to the mechanism that the incoming photon couples with a $q\bar{q}$ pair which interacts with the nucleon by the Pomeron exchange before forming the outgoing vector meson. The quark-Pomeron vertex is obtained by the Pomeron-photon analogy [8], which treats the Pomeron as a $C = +1$ isoscalar photon, as suggested by a study of nonperturbative two-gluon exchanges [22]. Following the formula given explicitly in Ref. [28], we then have

$$\mathcal{M}_\mathbb{P}^{\mu\nu}(p',p) = G_\mathbb{P}(s,t)\mathcal{T}_\mathbb{P}^{\mu\nu}(p',p) \quad (3)$$

with

$$\mathcal{T}_\mathbb{P}^{\mu\nu}(p',p) = i12\sqrt{4\pi\alpha_{\text{em}}}\frac{M_V^2\beta_q\beta_{q'}}{f_V}\frac{1}{M_V^2 - t}$$
$$\times \left(\frac{2\mu_0^2}{2\mu_0^2 + M_V^2 - t}\right)F_1(t)\{\not{q}g^{\mu\nu} - q^\mu\gamma^\nu\}, \quad (4)$$

where $t = (p - p')^2, s = (q + p)^2 = W^2, \alpha_{\text{em}} = e^2/4\pi, \beta_q$ is the Pomeron-quark coupling constant, M_V is the vector-meson mass, and $F_1(t)$ is the isoscalar electromagnetic form factor of the nucleon,

$$F_1(t) = \frac{4M_N^2 - 2.8t}{(4M_N^2 - t)(1 - t/0.71)^2}. \quad (5)$$

Here t is in unit of GeV^2, and M_N is the proton mass.

The Regge propagator for the Pomeron in Eq. (3) is

$$G_\mathbb{P} = \left(\frac{s}{s_0}\right)^{\alpha_P(t)-1}\exp\left\{-\frac{i\pi}{2}[\alpha_P(t) - 1]\right\}, \quad (6)$$

where $\alpha_P(t) = \alpha_0 + \alpha_P't$. It is common [28] to use $\alpha_0 = 1.08$ and $\alpha_P' = 1/s_0 = 0.25$ GeV^{-2}. In Eq. (4), f_V is the vector-meson decay constant: $f_\rho = 5.33, f_\omega = 15.2, f_\phi = 13.4$, and

$f_{J/\Psi} = 11.2$. The other parameters in Eq. (4) have been determined by fitting [28] the total cross section data of the photoproduction of ρ and ω: $\beta_u = \beta_d = 2.07$ GeV^{-1} and $\mu_0^2 = 1.1$ GeV^2.

With the parameters specified above, our task is to examine the extent to which the total cross section of photoproduction of J/Ψ can be fitted by only adjusting the Pomeron-charmed quark coupling constant β_c. This will be discussed in Sec. IV.

B. Pion-exchange amplitude

We observe from the Particle Data Group [27] that the width of the $J/\Psi \to \pi^0 \rho^0$ is significant,

$$\Gamma_{J/\Psi \to \pi^0 \rho^0} = 0.92 \text{ MeV} \times (0.56 \pm 0.07)\%. \quad (7)$$

With the vector-meson dominance (VDM) assumption, this experimental information allows us to calculate the one-pion-exchange amplitude of $\gamma + N \to J/\Psi + N$, as illustrated in Fig. 1(b), by using the following Lagrangian:

$$L = L_{J/\Psi,\rho^0\pi^0} + L_{\pi NN} + L_{VDM} \quad (8)$$

with

$$L_{J/\Psi,\rho^0\pi^0} = -\frac{g_{J/\Psi,\rho^0\pi^0}}{m_{J/\Psi}} \epsilon^{\mu\nu\alpha\beta} \partial_\mu \rho^0{}_\nu \partial_\alpha \phi_{J/\Psi,\beta} \phi_{\pi^0}, \quad (9)$$

$$L_{\pi NN} = -\frac{f_{\pi NN}}{m_\pi} \bar{\psi}_N \gamma_\mu \gamma_5 \vec{\tau} \psi_N \partial^\mu \cdot \vec{\phi}_\pi, \quad (10)$$

$$L_{VDM} = \frac{e m_\rho^2}{f_\rho} A^\mu \rho_\mu^0, \quad (11)$$

where ρ_μ^0, $\phi_{J/\Psi,\beta}$, $\vec{\phi}_\pi$, A^μ, and ψ_N are the field operators for ρ^0, J/Ψ, π, photon (γ), and nucleon (N), respectively. The mass for particle a is denoted as m_a. The well-determined coupling constants are $f_{\pi NN}^2/4\pi = 0.079$, $e^2/4\pi = 1/137$, and $f_\rho = 5.33$. To determine $g_{J/\Psi,\rho^0\pi^0}$, we use $L_{J/\Psi,\rho^0\pi^0}$ given in Eq. (9) to calculate the decay width

$$\Gamma_{J/\Psi \to \pi^0 \rho^0} = (2\pi)\frac{1}{3}\sum_{\lambda_\rho, \lambda_{J/\Psi}} \int d\Omega_k |\langle \vec{k}\lambda_\rho|H|\vec{p}=0, \lambda_{J/\Psi}\rangle|^2$$
$$\times \frac{k E_\pi(k) E_\rho(k)}{m_{J/\Psi}}, \quad (12)$$

where k is defined by $m_{J/\Psi} = E_\pi(k) + E_\rho(k)$, and

$$\langle \vec{k}\lambda_\rho|H|\vec{p}, \vec{\lambda}_{J/\Psi}\rangle$$
$$= \frac{1}{(2\pi)^{3/2}} \frac{1}{\sqrt{2E_{J/\Psi}(p)}} \frac{1}{\sqrt{2E_\rho(k)}} \frac{1}{\sqrt{2E_\pi(k)}} \frac{-g_{J/\Psi\rho^0\pi^0}}{m_{J/\Psi}}$$
$$\times \epsilon^{\mu\nu\alpha\beta} k_\mu^\rho \epsilon_{\nu,\lambda_\rho}(k^\rho) p_\alpha \epsilon_{\beta,\lambda_{J/\Psi}}(p) \left[\frac{\Lambda_{J/\Psi}^2}{(\vec{k}^2 + \Lambda_{J/\Psi}^2)}\right]^2. \quad (13)$$

Here we have included a dipole cutoff function with a range parameter $\Lambda_{J/\Psi}$. The four-momenta are defined in the rest frame of J/Ψ:

$$p = (m_{J/\Psi}, \vec{0}),$$
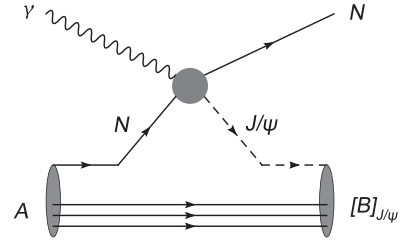$$k^\rho = (E_\rho(k), \vec{k}),$$
$$k^\pi = (E_\pi(k), -\vec{k}).$$

FIG. 2. The impulse approximation mechanism of $\gamma + A \to N + [B]_{J/\Psi}$ reaction. A is a nucleus with mass number A and B could be a nucleus with mass number $(A-1)$ or a $[q^{3(A-1)}]$ multiquark cluster.

By using Eqs. (12)–(13) and the experimental value given in Eq. (7), we find $g_{J/\Psi,\pi^0\rho^0} = 0.032$ for a cutoff $\Lambda_{J/\Psi} = 2000$ MeV.

With the Lagrangian Eq. (8), the one-pion-exchange invariant amplitude for $\gamma(q) + N(p) \to J/\Psi(k) + N(p')$ can be written as

$$I_{fi} = \bar{u}_{m'_s}(p')\epsilon_\mu^*(k, \lambda_{J/\Psi}) M_\pi^{\mu\nu}(p', p)\epsilon_\nu(q, \lambda_\gamma) u_{m_s}(p) \quad (14)$$

with

$$M_\pi^{\mu\nu}(p', p) = G \times F(t) \frac{1}{t - m_\pi^2} \epsilon^{\mu\nu\alpha\beta} k_\alpha q_\beta [\gamma \cdot (p' - p)]\gamma^5, \quad (15)$$

where $t = (p - p')^2$, and

$$G = \frac{e}{f_\rho} \frac{g_{J/\Psi,\rho^0\pi^0}}{m_{J/\Psi}} \frac{f_{\pi NN}}{m_\pi}, \quad (16)$$

$$F(t) = F_{\pi NN}(t) F_{J/\Psi,\rho^0\pi^0}(t). \quad (17)$$

Here we have introduced a cutoff form factor $F(t)$ to regularize the interaction vertices. For simplicity, we use the following form:

$$F(t) = \left(\frac{\Lambda^2}{\Lambda^2 - t}\right)^n. \quad (18)$$

We set $n = 4$, and $\Lambda = \Lambda_{J/\Psi} = 2000$ MeV.

III. PHOTOPRODUCTION OF $[B]_{J/\Psi}$ BOUND STATE

A. Reaction mechanism

With the impulse approximation, we assume that a J/Ψ is produced on a nucleon in the target nucleus A and then is attracted by a spectator system B to form a bound state $[B]_{J/\Psi}$. For simplicity, $[B]_{J/\Psi}$ is denoted as d in the following formula.

With the mechanism illustrated in Fig. 2, the cross section of $\gamma(\vec{q}) + A(-\vec{q}) \to N(\vec{p}) + d(-\vec{p})$ in the center-of-mass system can be written as

$$\frac{d\sigma}{d\Omega} = \left[\frac{(2\pi)^4 E_A(q)}{W}\right]\left[\frac{p E_N(p) E_d(p)}{W}\right]\frac{1}{2}\frac{1}{2J_A + 1}$$
$$\times \sum_{\lambda, M_{J_A}} \sum_{m_s, m_d} |\langle \vec{p}m_s, \Psi_{j_d M_d}|T(W)|\vec{q}\lambda, \Phi_{J_A, M_{J_A}}^A\rangle|^2, \quad (19)$$

where

$$
\langle \vec{p}m_s, \Psi_{j_d M_d} | T(W) | \vec{q}\lambda, \Phi^A_{J_A, M_{J_A}} \rangle = \sum_{j,m_j} \sum_{j_\alpha, m_{j_\alpha}} \langle \Psi_{j_d M_d} | a^\dagger_{jm_j} b_{j_\alpha, m_{j_\alpha}} | \Phi^A_{J_A, M_{J_A}} \rangle
$$

$$
\times \left[\sum_{m_{J/\Psi}, m_{s_\alpha}} \int d\vec{k} \chi^*_{j,m_j}(\vec{Q}_d, m_{J/\Psi}) \langle \vec{p}m_s, \vec{k}m_{J/\Psi} | t(W) | \vec{q}\lambda, \vec{p}_\alpha m_{s_\alpha} \rangle \phi_{j_\alpha, m_{j_\alpha}}(\vec{Q}_A, m_{s_\alpha}) \right]. \tag{20}
$$

Here $a^\dagger_{jm_j}$ is the creation operator for a J/Ψ with wave function $\chi_{j,m_j}(\vec{Q}_d, m_{J/\Psi})$, $b_{j_\alpha, m_{j_\alpha}}$ an annihilation operator for a nucleon with wave function $\phi_{j_\alpha, m_\alpha}(\vec{Q}_A, m_{s_\alpha})$, and the $\gamma + N \rightarrow J/\Psi + N$ amplitude is

$$
\langle \vec{p}m_s, \vec{k}m_{J/\Psi} | t(W) | \vec{q}\lambda, \vec{p}_\alpha m_{s_\alpha} \rangle = \frac{1}{(2\pi)^3} \frac{1}{\sqrt{2E_{J/\Psi}(k)}} \sqrt{\frac{m_N}{E_N(p_\alpha)}} \frac{1}{\sqrt{2q}} \sqrt{\frac{m_N}{E_N(p)}}
$$

$$
\times \left[\bar{u}_{m_s}(p) \epsilon^*_\mu(k, m_{J/\Psi}) \{ M^{\mu\nu}_\pi(p, p_\alpha) + \mathcal{M}^{\mu\nu}_\mathbb{P}(p, p_\alpha) \} \epsilon_\nu(q, \lambda) u_{m_{s_\alpha}}(p_\alpha) \right], \tag{21}
$$

where $M^{\mu\nu}_\pi$ is the pion-exchange amplitude given in Eq. (15), and $\mathcal{M}^{\mu\nu}_\mathbb{P}$ is the Pomeron-exchange amplitude in Eq. (3).

For simplicity, we will only perform calculations for the reactions on ^{3}He and ^{4}He. For estimations of cross sections on these target nuclei, it is sufficient to use the s-wave harmonic oscillator wave functions for both the target A and B in the $[B]_{J/\Psi}$ bound state. We also only consider the case that the J/Ψ in the produced bound $B_{J/\Psi}$ is on an s-wave orbital. For the case $B = A - 1$ nuclear system, we thus write the initial ($|\Phi^A\rangle$) and final ($|\Psi\rangle$) nuclear states as

$$
|\Phi^A\rangle = [|N\rangle \otimes |\Phi^{A-1}\rangle]_{L=0}, \tag{22}
$$

$$
|\Psi\rangle = [|J/\Psi\rangle \otimes |\Phi^{A-1}\rangle]_{L=0}, \tag{23}
$$

where L is the relative angular momentum between N or J/Ψ and the $(A-1)$ nucleus. Explicitly, we have

$$
|\Phi^A_{J_A, M_{J_A}}\rangle = \sum_{M_{J_{A-1}}} \sum_{j_\alpha, m_{j_\alpha}} \langle J_A M_{J_A} | j_\alpha J_{A-1} m_{j_\alpha} M_{J_{A-1}} \rangle b^\dagger_{j_\alpha m_{j_\alpha}} |\Phi^{A-1}_{J_{A-1}, M_{J_{A-1}}}\rangle,
$$

$$
|\Psi_{J_d, M_d}\rangle = \sum_{M_{J_{A-1}}} \sum_{j,m_j} \langle J_d M_d | j J_{A-1} m_j M_{J_{A-1}} \rangle a^\dagger_{jm_j} |\Phi^{A-1}_{J_{A-1}, M_{J_{A-1}}}\rangle. \tag{24}
$$

Then the momentum variables in Eqs. (20) and (21) are

$$
\vec{p}_\alpha = \vec{p} + \vec{k} - \vec{q}, \tag{25}
$$

$$
\vec{p}_\beta = -\vec{p} - \vec{k} = -\vec{q} - \vec{p}_\alpha, \tag{26}
$$

$$
\vec{Q}_A = \frac{\vec{p}_\alpha E_{A-1}(\vec{p}_\beta) - \vec{p}_\beta E_N(\vec{p}_\alpha)}{E_{A-1}(\vec{p}_\beta) + E_N(\vec{p}_\alpha)}, \tag{27}
$$

$$
\vec{Q}_d = \frac{\vec{k} E_{A-1}(\vec{p}_\beta) - \vec{p}_\beta E_{J/\Psi}(\vec{k})}{E_{J/\Psi}(\vec{k}) + E_{A-1}(\vec{p}_\beta)}, \tag{28}
$$

where $\vec{Q}_d$ ($\vec{Q}_A$) is the relativistic relative momentum between J/Ψ (N) and the $(A-1)$ nuclear system.

For the target ^{4}He, we have $J_A = 0$ and assume that $|\Phi^{A-1}_{J_{A-1}, M_{J_{A-1}}}\rangle$ is the ^{3}He ground state with $J_{A-1} = 1/2$. We then have the following simplicities:

$$
\langle \Psi_{j_d M_d} | a^\dagger_{jm_j} b_{j_\alpha, m_{j_\alpha}} | \Phi^A_{J_A, M_{J_A}} \rangle = \langle J_A M_{J_A} | j_\alpha J_{A-1} m_{j_\alpha} M_{J_{A-1}} \rangle \langle J_d M_d | j J_{A-1} m_j M_{J_{A-1}} \rangle
$$

$$
\rightarrow \frac{1}{\sqrt{2}} \langle J_d M_d | j_\alpha j - m_{j_\alpha} m_j \rangle, \tag{29}
$$

and

$$
\chi_{j,m_j}(\vec{Q}_d, m_{J/\Psi}) = \delta_{j,1} \delta_{m_j, m_{J/\Psi}} \frac{1}{\sqrt{4\pi}} F(Q_d), \tag{30}
$$

$$
\phi_{j_\alpha, m_{j_\alpha}}(\vec{Q}_A, m_{s_\alpha}) = \delta_{j_\alpha, 1/2} \delta m_{j_\alpha}, \quad m_{s_\alpha} \frac{1}{\sqrt{4\pi}} R(Q_A), \tag{31}
$$

Eq. (20) then becomes

$$\langle \vec{p} m_s, \Psi_{j_d M_d} | T(W) | \vec{q} \lambda, \Phi^A_{J_A, M_{J_A}} \rangle = \sum_{M_{J_{A-1}}} \sum_{m_{J/\Psi}, m_{s_\alpha}} \langle J_A M_{J_A} | j_\alpha J_{A-1} m_{j_\alpha} M_{J_{A-1}} \rangle \langle J_d M_d | j J_{A-1} m_j M_{J_{A-1}} \rangle$$

$$\times \left[\int d\vec{k} \frac{1}{\sqrt{4\pi}} F(Q_d) \langle \vec{p} m_s \vec{k} m_{J/\Psi} | t(W) | \vec{q} \lambda, \vec{p}_\alpha m_{s_\alpha} \rangle \frac{1}{\sqrt{4\pi}} R(Q_A) \right]. \quad (32)$$

We have applied the formula Eqs. (19) and (32) to estimate the production cross section on ^{4}He. We use the usual s-wave harmonic oscillator wave function with $b = 1.32$ fm for the target ^{4}He

$$R(p) = \left[N e^{\frac{-b^2 p^2}{2}} \right] \quad (33)$$

with the normalization $\int R^2(p) p^2 dp = 1$. For the J/Ψ wave function in $d = [^3\text{He}]_{J/\Psi}$, we will generate an s-wave $\psi_{J/\Psi}(r)$ from a potential $V_{J/\Psi, B}(r)$ with the normalization $\int r^2 dr |\psi_{J/\Psi}(r)|^2 = 1$. The wave function in Eq. (30) and also in Eq. (32) can then be calculated from

$$F(p) = \int_0^\infty r^2 dr j_0(pr) \psi_{J/\Psi}(r), \quad (34)$$

where $j_0(z)$ is the spherical Bessel function. The form of $V_{J/\Psi, B}(r)$ will be discussed in Sec. IV.

The above formula can be easily extended to investigate other possible impulse approximation mechanisms as far as all wave functions in the bound A and $[B]_{J/\Psi}$ are all in s waves. This is what we will need in Sec. IV when we consider the production of $[q^6]_{J/\Psi}$ from the q^6-N component of ^{3}He.

IV. RESULTS

A. Models of $\gamma + N \rightarrow J/\Psi + N$ reaction

We first develop a model consisting of Pomeron-exchange and pion-exchange mechanisms, as described in Sec. II. With the parameters specified there, we try to fit the available total cross section data of $\gamma + p \rightarrow J/\Psi + p$ up to invariant mass $W = 300$ GeV by only adjusting the charmed quark-Pomeron coupling constant β_c. With $\beta_c = 1.21$ we only able to fit the data up to 20 GeV. Clearly, the result at high energy is not satisfactory as shown in the red dashed curve in the left-hand side of Fig. 3. We then find that by changing α_0 of the Regge trajectory in the Pomeron propagator Eq. (6) from $\alpha_0 = 1.08$, as determined in the previous fits [28] to the total cross sections of ρ and ω photoproduction, to $\alpha_0 = 1.25$, we are able to get a very good fit to the data by choosing $\beta_c = 0.84$ GeV^{-1}. Our fit is the solid black curve in the left-hand side of Fig. 3. We thus will use the model with $\alpha_0 = 1.25$ and $\beta_c = 0.84$ GeV^{-1} (PM model) in our investigations. As also seen in the insert in the left-hand side of Fig. 3, the contribution (magenta dotted curve) from the pion-exchange amplitude, as defined by Eqs. (14)–(18), is very weak except in the very near threshold region.

We next consider the model of Ref. [13] based on the two-gluon ($2g$) and three-gluon ($3g$) exchange mechanisms. In terms of the normalization defined by Eq. (2), the amplitude of this model can be written as

$$\langle \vec{k} \lambda_{J/\psi} m_s' | t(W) | \vec{q} \lambda_\gamma m_s \rangle$$

$$= \frac{1}{(2\pi)^3} \frac{1}{\sqrt{2 E_{J/\psi}(k)}} \sqrt{\frac{m_N}{E_N(k)}} \sqrt{\frac{m_N}{E_N(q)}} \frac{1}{\sqrt{2q}}$$

$$\times \frac{4\sqrt{\pi}}{\sqrt{6}} \frac{q w}{m_N} [\mathbf{M}_{2g} + \mathbf{M}_{3g}] \quad (35)$$
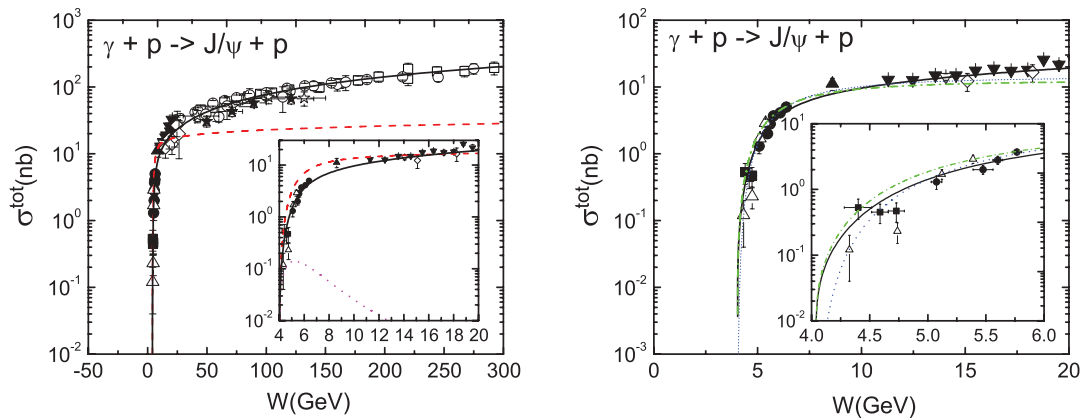

FIG. 3. (Color online) The total cross section of the $\gamma + p \rightarrow J/\psi + p$ reaction as function of the γp invariant mass W. Left: The black solid and red dashed are the results from using ($\alpha_0 = 1.25$, $\beta_c = 0.84$ GeV^{-1}; called the PM model) and ($\alpha_0 = 1.08$, $\beta_c = 1.21$ GeV^{-1}) within the model which include both the π-exchange and Pomeron-exchange mechanisms. The magenta dotted curve in the insert is the contribution from the π exchange. Right: The black solid, blue dotted, and green dot-dashed lines are from the PM model, the $2g$ model of Ref. [13], and the $2g + 3g$ model based on Eq. (35). The experimental data are from [30–38].

with

$$\mathbf{M}_{2g} = \frac{A_{2g}}{4\sqrt{\pi}} \frac{1-x}{R m_{J/\psi}} e^{bt/2}, \tag{36}$$

$$\mathbf{M}_{3g} = \frac{A_{3g}}{4\sqrt{\pi}} \frac{1}{R^2 m_{J/\psi}^2} e^{bt/2}, \tag{37}$$

$$x = \frac{2 m_N m_{J/\psi} + m_{J/\psi}^2}{W^2 - m_p^2}, \tag{38}$$

where $R = 1$ fm, $b = 1.13$ GeV^{-2} are taken from Ref. [13]. We follow Ref. [13] to determine the parameters A_{2g} and A_{3g} by fitting the data up to only 20 GeV. In the two-gluon-exchange model ($2g$), we set $A_{3g} = 0$ and obtain $A_{2g} = 0.028$ MeV^{-2} from the fit. In the $2g + 3g$ model, the fit is obtained by choosing $A_{2g} = 0.023$ MeV^{-2} and $A_{3g} = 2000$ MeV^{-2}. The fits for the $2g$ and $2g + 3g$ models are the dotted and dot-dashed curves in the right-hand side of Fig. 3, respectively. Clearly, they have differences with that (black solid) of the PM model, as can be seen more clearly in the insert in the right-hand side of Fig. 3. Here we also see that the data in the region near the J/ψ production threshold are very limited and uncertain. We will therefore perform calculations using the PM, $2g$, and $2g + 3g$ models to examine the model dependence of our predictions. Clearly, precise data in the near threshold region are needed to make progress.

B. Photoproduction of J/Ψ-nucleus bound states

Following the previous investigations [7,29], we assume that the interaction between a J/Ψ and a nucleus with mass number A can be parametrized as a nonrelativistic potential of the following Yukawa form:

$$V_{J/\Psi,A}(r) = -\alpha_A \frac{e^{-\mu_A r}}{r}. \tag{39}$$

There exists two different approaches to determine the parameters α_A and μ_A for the nucleon with $A = 1$. We will explain these in the following two subsections.

1. Pomeron-quark coupling model

Motivated by the previous studies in quantum electrodynamics, it is assumed in the approach of Ref. [7] that the J/Ψ-A forward angle scattering amplitude at very high energy can be related to the matrix element of the potential Eq. (39) which is understood to be valid only in the region where J/Ψ moves nonrelativistically. They further assume that the J/Ψ-A amplitudes can be calculated by using the Pomeron-exchange model of Dannachie and Landshoff [8]. In the very high energy approximation, the differential cross section of J/Ψ-A elastic scattering can be related to the parameters α_A and μ_A of the potential Eq. (39) by the following relation:

$$\frac{d\sigma}{dt}(J/\Psi\, A \to J/\Psi\, A) = \frac{[2\beta_c F_{J/\Psi}(t)]^2 [3A\beta_{u/d} F_A(t)]^2}{4\pi} \tag{40}$$

$$= \frac{4\pi \alpha_A^2}{(-t + \mu_A^2)^2}, \tag{41}$$

TABLE I. Parameters for determining the potential Eq. (39) using the Pomeron-quark coupling model defined by Eqs. (41)–(43). The predicted binding energies (B.E.) for proton ($A = 1$), ^{3}He ($A = 3$), and ^{12}C ($A = 12$) are also listed.

A	$\langle R_A^2 \rangle^{1/2}$ (GeV^{-1})	μ_A (GeV)	$\beta_{u/d}$ (GeV^{-1})	β_c (GeV^{-1})	α_A	B.E. (MeV)
1	3.9	0.63	1.85	1.85	0.64	–
			2.05	1.21	0.47	–
			2.05	0.84	0.33	–
3	9.5	0.26	1.85	1.85	0.33	19.86
			2.05	1.21	0.23	3.27
			2.05	0.84	0.16	0.04
12	12.69	0.19	1.85	1.85	0.73	280.0
			2.05	1.21	0.53	165.0
			2.05	0.84	0.37	67.0

where t is the momentum-transfer squared, $\beta_{u/d}$ (β_c) is the Pomeron coupling with the $up/down(charmed)$ quarks, $F_{J/\Psi}(t)$ and $F_A(t)$ are the form factors for J/Ψ and the nucleus with mass number A, respectively. They further assume that in the $t \to 0$ limit, the slope of $d\sigma/dt$ is mainly determined by $dF_A(t)/dt$ and that $F_A(t)$ can be identified with the nuclear electromagnetic form factor. One then gets the following relations:

$$\mu_A^{-2} = \left| \frac{dF_A(t)}{dt} \right|_{t=0} = \frac{\langle R_A^2 \rangle}{6}, \tag{42}$$

$$\alpha_A = \frac{[2\beta_c][3A\beta_{u/d}]}{4\pi} \mu_A^2. \tag{43}$$

The radius $\langle R_A^2 \rangle^{1/2}$ can be taken from Ref. [39]. The Pomeron-quark coupling constants can be taken from fits to the data of meson-nucleon scattering or photoproduction of vector mesons. Once α_A and μ_A of the potential Eq. (39) are determined, we can predict the possible J/Ψ-nucleus bound states. In Table I, we list our results for proton ($A = 1$), ^{3}He ($A = 3$) and ^{12}C ($A = 12$) for various sets of Pomeron-quark coupling constants. The first rows in the results for each A are based on the flavor independent $\beta_{u/d} = \beta_c = 1.85$ GeV^{-1} of Ref. [7]. The other two results use the Pomeron-quark coupling constants $\beta_{u/d} = 2.05$ GeV^{-1} determined [28] in the fits to the data of photoproduction of ρ and ω, and β_c determined from the fits described in Sec. IV A.

With the determined potential parameters α_A and μ_A, the predicted binding energies ($B.E.$) for each considered nuclear system are listed in the last column of Table I. For the $A = 1$ case, we see that there is no J/Ψ-N bound state. But all three models predict bound $[^3\text{He}]_{J/\Psi}$ and $[^{12}\text{C}]_{J/\Psi}$ states. In the left-hand side of Fig. 4, we show the predicted cross sections of $\gamma + {^4}\text{He} \to [^3\text{He}]_{J/\Psi} + n$. Clearly, the predicted cross sections depend on the Pomeron-quark coupling constants. Furthermore, their magnitudes depend sensitively on the binding energy (B.E.) of the predicted $[^3\text{He}]_{J/\Psi}$ system. As the binding energy decreases from 19.86 MeV to 0.04 MeV, the predicted cross sections drop by two orders in magnitude. This can be understood from the right-hand side of Fig. 4 where we compare the J/Ψ-^{3}He relative wave functions which are used
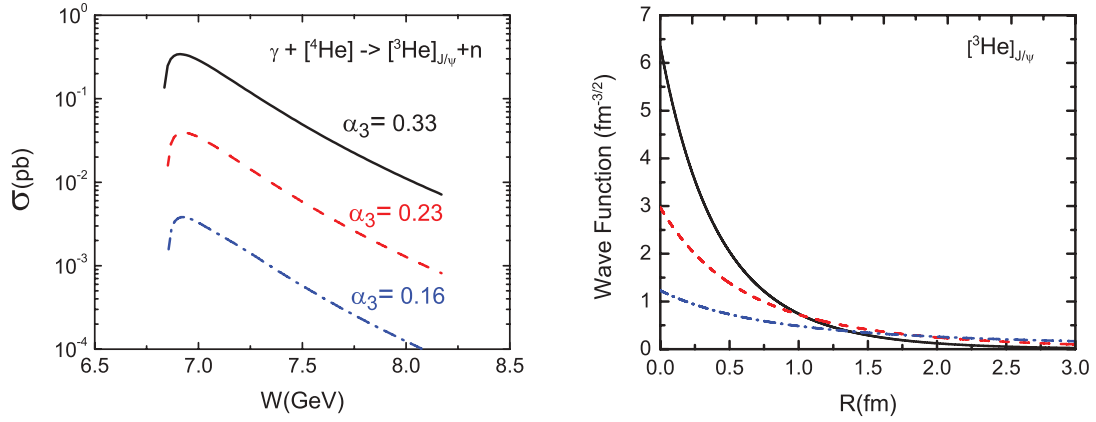
FIG. 4. (Color online) The total cross section of $\gamma + [^4\text{He}] \rightarrow {}^3\text{He}_{[J/\psi]} + n$ as function of γ-^{4}He invariant mass W (left) and the wave function (right) for $J/\psi - {}^3$He system. The black solid, red dashed, and blue dotted-dashed lines are calculated by using the potential Eq. (39) with $A = 3$, $\mu_A = 0.257$ GeV, and $\alpha_A = 0.33, 0.23, 0.16$, respectively.

in predicting the cross sections in the left-hand side. We see that the wave function (solid black) for B.E. = 19.86 MeV is much shorter range than the other two cases and hence gives more cross sections in this large momentum-transfer reaction. This is explicitly illustrated in Fig. 5 where we show that the cross section (red dashed curve) calculated from keeping only the high momentum part ($p_{J/\psi} > 1400$ MeV) of the J/ψ wave function in the integration in Eq. (32) is very close to the full calculation (solid black curve).

In Fig. 6, we see that the predicted differential cross sections are forward peaked, as expected from the Pomeron-exchange mechanism. In Fig. 7, we show that the predicted cross sections depend on the $\gamma + N \rightarrow J/\psi + N$ model. Their maximum values are, however, comparable ~ 0.1–0.3 pb. Clearly, it is important to get accurate data of $\gamma + N \rightarrow J/\psi + N$ at low energies to refine the employed model for making more precise predictions.

The $[^{12}\text{C}]_{J/\psi}$ can be produced by $\gamma + {}^{13}\text{C} \rightarrow [^{12}\text{C}]_{J/\psi} + n$. However, making predictions for the cross sections of this process is beyond the scope of this paper since the simple

s-wave description of the nuclei in Sec. III is no longer a reasonable approximation for nuclei heavier than ^{4}He.

2. Folding model

While all three J/ψ-N models listed in Table I do not have bound states, there exist a possibility that adding the J/ψ-N interactions from the nucleons in a nucleus could lead to bound states. To explore this possibility, we follow the usual nuclear physics approach to construct a folding potential for the interaction between a J/ψ and a nuclear system:

$$V_{J/\psi,A}(r) = \int v_{J/\psi,N}(\vec{r} - \vec{r}\,')\rho_A(\vec{r}\,')d\vec{r}\,', \qquad (44)$$

where $v_{J/\psi,N}(r) = V_{J/\psi,1}(r)$ as defined by Eq. (39) with $A = 1$, and the nuclear density is normalized by

$$\int \rho_A(\vec{r}\,')d\vec{r}\,' = A. \qquad (45)$$

For ^{3}He we use $\rho_A(\vec{r}) = \rho_0 e^{-r^2/b^2}$ with $b = 1.32$ fm which is obtained by fitting the ^{3}He charge form factor at low momentum-transfer. For heavy nuclei, we use the
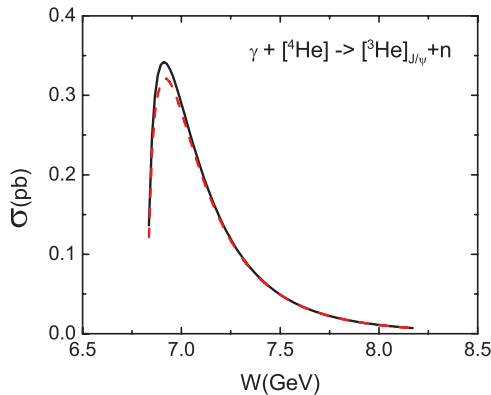

FIG. 5. (Color online) The cross section of $\gamma + [^4\text{He}] \rightarrow [^3\text{He}]_{[J/\psi]} + n$ as function of γ-^{4}He invariant mass W. The red dashed curve is obtained from keeping only the contribution from the J/ψ wave function with $k > 1400$ MeV in the integration of Eq. (32).

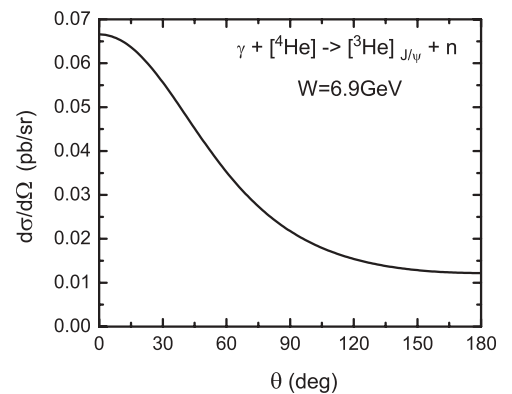

FIG. 6. The differential cross section of $\gamma + [^4\text{He}] \rightarrow [^3\text{He}]_{[J/\psi]} + n$ vs the angle of out going N with the center mass 6.9 GeV.
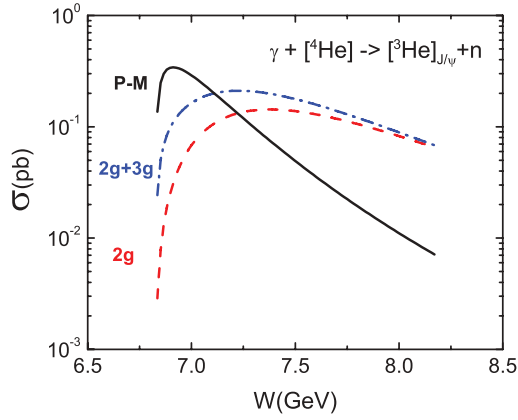
FIG. 7. (Color online) The total cross section of $\gamma + [^4\text{He}] \rightarrow [^3\text{He}]_{[J/\psi]} + n$ vs the certain mass of system. The black solid, red dashed, and blue dot-dashed lines are for the Pomeron and π exchange, Brodsky's $2g$ model, and $2g + 3g$ model, respectively.

Woods-Saxon form [40]

$$\rho_A(\vec{r}) = \rho_0 \frac{1}{1 + e^{(r-R)/t}} \qquad (46)$$

with $R = 1.1 A^{-1/3}$ fm and $t = 0.53$ fm.

Our results using the parameters of Ref. [7] to calculate $v_{J/\Psi,N}(\vec{R})$ in Eq. (44) are listed in the first row of Table II. We see that the folding model gives 1.62 MeV (7.0 MeV) for $[^3\text{He}]_{J/\psi}([^{12}\text{C}]_{J/\psi})$ which are much less than 19.86 MeV (280 MeV) listed in Table I. The predicted cross sections for $\gamma + {}^4\text{He} \rightarrow [^3\text{He}]_{J/\psi} + n$ are also found to be much weaker, close to the blue dot-dashed curve ($\alpha_3 = 0.16$) in Fig. 4. Clearly, it is difficult to measure such a loosely bound $[^3\text{He}]_{J/\psi}$ state.

To examine the model dependence, we also consider folding potentials by using three other J/Ψ-N models. Two [4,6] of them are constructed by using the results from the heavy quark effective field theory calculation by Peskin [1]. The third one [5] is from lattice QCD calculation. Their results can also be written in the Yukawa form of Eq. (39) with $A = 1$. We find that these three models do not generate a $[^3\text{He}]_{J/\psi}$ bound state as indicated in Table II. For ^{12}C, the binding energies from folding model are much weaker than those listed in Table I from the Pomeron-quark coupling model.

TABLE II. The binding energy of J/ψ-nucleus calculated with the folding potential defined by Eq. (44) with parameters of $v_{J/\Psi,N} = -\alpha_1 \frac{e^{-\mu_1 r}}{r}$ taken from different references. The parameters of Ref. [4] are obtained from reproducing the scattering length $a = -0.24$ fm given in Ref. [4]. (A Gaussian form of the $v_{J/\Psi,N}$ was used in Ref. [4].)

Model	Parameter (MeV)		Binding energy (MeV)		
	α_1	μ_1 (GeV)	$[H]_{J/\psi}$	$[^3\text{He}]_{J/\psi}$	$[^{12}\text{C}]_{J/\psi}$
Ref. [7]	0.64	0.63	–	1.62	7.0
Ref. [4]	0.20	0.63	–	–	0.91
Ref. [5]	0.10	0.63	–	–	0.003
Ref. [6]	0.06	0.63	–	–	–

C. Photoproduction J/Ψ-(q^6) bound states

In Ref. [13], it was suggested that a $c\bar{c}$ system could interact strongly with the color octet three-quark $[\bar{q}^3]_8$ component of the six-quark cluster ($[q^6] = [q^3]_8[\bar{q}^3]_8$) which could dominant the short-range part of the deuteron wave function. The possible attractive force between a J/Ψ and a six-quark cluster was suggested in the study of Ref. [12] where the excitation of a hidden charm $|qqqqqc\bar{c}\rangle$ state is introduced to explain the spin correlation of pp elastic scattering near the J/Ψ production threshold. Here we examine the condition under which a bound $[q^6]_{J/\Psi}$ color singlet state can be produced in the $\gamma + {}^3\text{He} \rightarrow [q^6]_{J/\Psi} + N$ reaction. Unlike the predictions for the photoproduction of $[^3\text{He}]_{J/\Psi}$ described in the previous subsection, very little information on $[q^6]$ and the $[q^6] - J/\Psi$ interaction is available. We thus need to make various assumptions which can only be considered to be plausible for estimating the production cross sections.

In the impulse approximation, as described in Sec. II, we need the initial N-$[q^6]$ wave function in ^3He and the final J/Ψ-$[q^6]$ wave function to calculate the cross section of $\gamma + {}^3\text{He} \rightarrow [q^6]_{J/\Psi} + N$. In the following subsections, we explain our procedure for modeling these two ingredients of our predictions.

1. Wave function of N-q^6 in ^3He

We start with a formulation of Refs. [18,42] within which the Hamiltonian for a two-nucleon system is written as

$$H = H_0 + v_{NN} + \sum_\alpha h_{[q^6]^\alpha \leftrightarrow NN}, \qquad (47)$$

where α denotes collectively the total angular momentum J, the total isospin T, and the parity P, and v_{NN} is a meson-exchange nucleon-nucleon (NN) interaction. The vertex interaction $h_{[q^6]^\alpha \leftrightarrow NN}$ defines the formation of a six-quark state $[q^6]^\alpha$ in NN collisions. The six-quark states $[q^6]^\alpha$ are identified with the states predicted by the Bag model calculations of Mulder [15]. By appropriately choosing the form of the vertex interaction $h_{[q^6]^\alpha \leftrightarrow NN}$, the NN scattering amplitudes derived from the Hamiltonian Eq. (47) are identical to those given by using the P-matrix approach of Jaffe and Low [14] and the compound bag model formulation developed in Refs. [16,17].

We will make use of the results of Fasano and Lee [18,19]. They determined the mass M_α of $[q^6]^\alpha$ cluster and the interaction $h_{[q^6]^\alpha \leftrightarrow NN}$ for $\alpha = {}^1S_0$ and $^3S_1$ by fitting the NN scattering phase shifts up to 1 GeV. Within the simple s-wave harmonic oscillator model for ^3He, the probabilities $P_{[q^6]^\alpha}$ of finding the $[q^6]^\alpha$-N in ^3He are estimated [19] to be $P_{[q^6]^{1}S_0} = 0.7\%$ and $P_{[q^6]^{3}S_1} = 0.06\%$. For simplicity, we neglect the small $^3S_1$ component. The bare mass of $[q^6]$ determined in Ref. [18] is $M_{^1S_0} = 2150$ MeV. Here we will use this information to model the relative wave function of $[q^6]^\alpha$-N which is needed to calculate the cross sections of $\gamma + {}^3\text{He} \rightarrow [q^6]_{J/\Psi} + N$.

We assume that the charge distribution in the region with the distance $r \leqslant r_c$ from the center of ^3He is completely due to $[q^6]^\alpha$-N components of the wave function. This is illustrated in Fig. 8. Each r_c clearly corresponds to a choice of P_{q^6}. Within
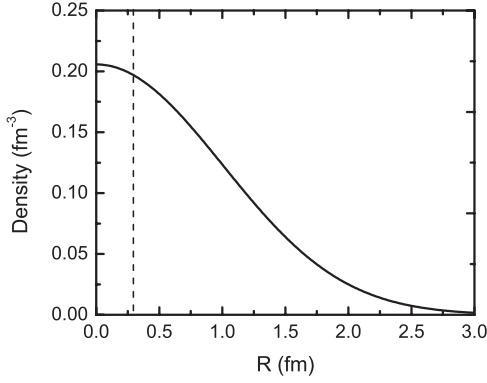
FIG. 8. The solid curve is the normalized density distribution calculated from using Eqs. (50) and (51) with $b = 1.35$ fm and $l_c = 0.5$ fm. The dashed line defines $r_c = 0.29$ fm for obtaining the probability $P_{[q^6]^1 S_0} = 0.7\%$ for finding the $[q^6] - N$ component in ^{3}He by using Eq. (53).

such a model, the charge form factor of ^{3}He is written as

$$F_c(Q^2) = F_c^{N^3}(Q^2) + F_c^{q^6-N}(Q^2). \tag{48}$$

We next observe that within the conventional nuclear model [41], the impulse approximation (IA) calculation, which includes only the one-body nucleon current, of $F_c(Q^2)$ is very close to the data in $Q^2 \leqslant$ about 10 fm^{-2} and can be reproduced very well by the Gaussian distribution of the s-wave harmonic oscillator wave function. The IA results from Ref. [41] in this Q^2 region are the solid squares in Fig. 9. We next demand that the s-wave three-nucleon wave function reproduce these IA results. In addition, the resulting $F_c(Q^2)$ in the higher Q^2 region must have the similar structure of IA up $Q^2 \sim 20$ fm^{-2} although we do not have higher partial wave components of the three-nucleon wave function. We achieve this by using the s-wave harmonic oscillator wave function with Jastrow two-body correlation used in Refs. [43,44]. We write

$$F_c(Q^2) = \int e^{-i\vec{Q}\cdot\vec{r}} \rho(\vec{r}) d\vec{r} \tag{49}$$
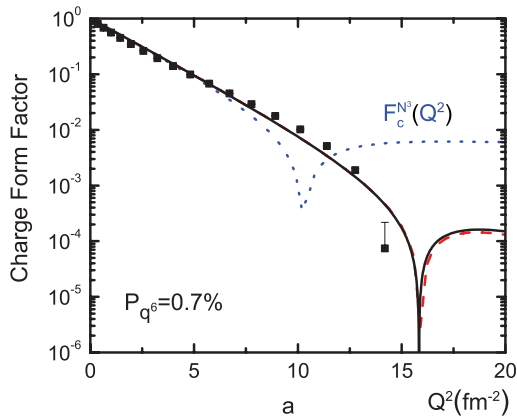
with

$$\rho(\vec{r}_1) = \int d\vec{r}_2 \rho_2(\vec{r}_1, \vec{r}_2), \tag{50}$$

where the two-body density is defined by

$$\rho_2(\vec{r}_1, \vec{r}_2) = N e^{-\frac{r_1^2 + r_2^2}{b^2}} \left(1 - e^{-\frac{|\vec{r}_1 - \vec{r}_2|^2}{2l_c^2}}\right),$$
$$N = \frac{1}{(\sqrt{\pi}b)^6} \frac{[l_c^2 + b^2]^{3/2}}{[l_c^2 + b^2]^{3/2} - l_c^3}. \tag{51}$$

As seen in Fig. 9, the solid black curve calculated with $b = 1.35$ fm and $l_c = 0.5$ fm can reproduce the impulse approximation calculation results (solid squares) given in Ref. [41] up to $Q^2 \sim 10$ fm^{-2}. At higher Q^2, the solid curves have the similar structure of the IA results. For our present s-wave calculations, we consider the solid curves in Fig. 9 as the $F_c(Q^2)$ in Eq. (48). Accordingly, the NNN contribution in Eq. (48) is calculated from

$$F_c^{N^3}(Q^2) = \int_{r_c}^{\infty} r^2 dr \int d\Omega_r e^{-i\vec{Q}\cdot\vec{r}} \rho(\vec{r}) \tag{52}$$

and the probability $P_{[q^6]}$ is defined by

$$P_{q^6} = \int_0^{r_c} r^2 dr \int d\Omega_r \rho(\vec{r}). \tag{53}$$

For $P_{q^6} = 0.7\%$ determined in Ref. [18] within the compound bag model of NN scattering, we choose $r_c = 0.292$ fm to calculate Eq. (52) and get the blue dotted curve in the left-hand side of Fig. 9. In the right-hand side, the blue dotted curve is from the calculation using Eq. (52) with $r_c = 0.630$ fm which gives $P_{q^6} = 6.3\%$. Clearly, both results agrees well with the IA (solid squares) and the solid curve only in the low Q^2 region. Our next task is to model $F^{q^6-N}(Q^2)$ such that for each r_c, $F_c(Q^2)$ (solid black curve) in Fig. 9 up to $Q^2 \sim 15$ fm^2 can be reproduced, as required by Eq. (48).
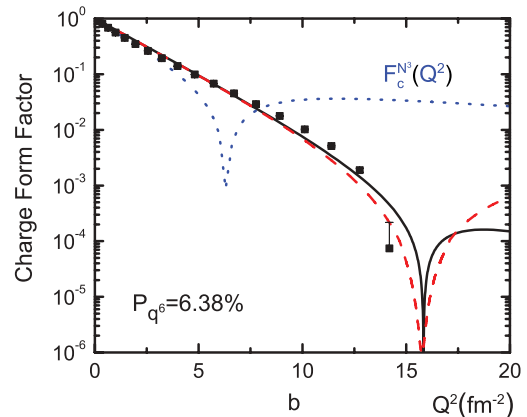

FIG. 9. (Color online) The charge form factor $F_c(Q^2)$ for ^{3}He. The solid squares are from the impulse approximation (IA) calculation of Ref. [41]. The dotted blue curves are $F_c^{N^3}(Q^2)$ calculated from using Eq. (52) with $r_c = 0.292$ fm and $P_{q^6} = 0.7\%$ (left) and $r_c = 0.630$ fm and $P_{q^6} = 6.3\%$ (right). The red dashed curves are from adding the $q^6 - N$ contributions calculated from using Eq. (54) with $b^* = 0.185$ fm (left) and $b^* = 0.414$ fm (right).

TABLE III. The parameters for ^6q-N and ^6q-J/ψ systems. See text for the explanations of the notations.

Model	q^6-N				q^6-J/ψ		
	P_{q^6}	r_c (fm)	b^* (fm)	$\langle r^2 \rangle^{1/2}$ (fm)	μ_{q^6} (GeV)	α_{q^6}	B.E. (MeV)
A_1	0.7%	0.292	0.185	0.226	0.6	1.33	498.42
A_2					1.0	1.50	389.63
B_1	4.0%	0.533	0.346	0.424	0.6	0.83	104.08
B_2					1.0	1.05	79.77
C_1	6.38%	0.630	0.414	0.507	0.6	0.75	65.84
C_2					1.0	0.97	51.33

For simplicity, we assume that $F_c^{q^6-N}(Q^2)$ can be calculated from a normalized Gaussian distribution

$$F_c^{q^6-N}(Q) = P_{q^6} \int e^{-i\vec{Q}\cdot\vec{r}} \left[\frac{1}{(\sqrt{\pi}b^*)^3} e^{\frac{-r^2}{b^{*2}}} \right] d\vec{r}. \quad (54)$$

Accordingly, the mean radius of q^6-N can be defined by

$$\langle r^2 \rangle = \int \left[\frac{1}{(\sqrt{\pi}b^*)^3} e^{\frac{-r^2}{b^{*2}}} \right] r^2 d\vec{r}. \quad (55)$$

We adjust b^* for each P_{q^6} to fit the solid curves in Fig. 9. We find that if P_{q^6} is larger than 6.5%, no b^* can fit the form factor defined by Eq. (48) in the $Q^2 < 20$ fm^{-2} region. In the cluster model of Ref. [21], $P_{q^6} = 4.0\%$ is obtained from fitting the ^{3}He form factor. The $P_{q^6} = 15\%$ determined in Ref. [20] by fitting the structure function of ^{3}He(e, e') is beyond what our formulation can accommodate. For comparison, we thus choose three different models with $P_{q^6} = 0.7\%$, 4%, and 6.38% for our calculations. In Table III, we list r_c, b^*, and also $\langle r^2 \rangle^{1/2}$ calculated from using Eq. (55) for these three cases. Our fits are the red dashed curves in Fig. 9 for $P_{q^6} = 0.7\%$ (left) and 6.38% (right).

Once b^* is determined, we then assume that the relative wave function of $[q^6]$-N can be described by the harmonic wave function with the same b^*. This should be reasonable for making order of magnitude estimates in this work. A more sophisticated approach should account for the quark charge distribution in $[q^6]$ which is beyond the scope of this work. Also, the sharp cutoff at $r = r_c$ to define $F_c^{N^3}$ in Eq. (52) should perhaps be better modeled. For our present qualitative estimations, this simple procedure should be sufficient.

2. Wave function of ^6q-J/ψ bound state

We follow the procedure of Sec. IV B to assume that the q^6-J/ψ bound states ($[q^6]_{J/\psi}$) are also defined by a potential of Yukawa form

$$V_{J/\Psi,q^6}(r) = -\alpha_{q^6} \frac{e^{-\mu_{q^6}r}}{r}. \quad (56)$$

We expect that if a $[q^6]_{J/\psi}$ bound state can be produced, its size must be small for color field to give strong attractive force. Thus it is reasonable to assume that the mean radius of $[q^6]_{J/\psi}$ is close to the value $\langle r^2 \rangle^{1/2}$ of the initial q^6-N system listed in Table III. We find that such a small size can be generated from

choosing $\mu_{q^6} > 0.6$ GeV in defining the potential Eq. (56). Once a value of μ_{q^6} is chosen, we then determine the potential strength α_{q^6} by requiring

$$\langle r^2 \rangle = \int |\phi_{q^6, J/\Psi}(\vec{r})|^2 r^2 d\vec{r}, \quad (57)$$

where $\phi_{q^6, J/\Psi}(\vec{r})$ is the J/Ψ-q^6 relative wave function generated from the potential Eq. (56), and the values of $\langle r^2 \rangle^{1/2}$ for various considered cases are listed in Table III. The resulting α_{q^6} and the binding energies (B.E.) are also listed there. Here we note that the binding energy increases as the mean radius $\langle r^2 \rangle^{1/2}$ and the corresponding probability P_{q^6} decrease.

3. The results of $\gamma + {}^3He \rightarrow [q^6]_{J/\psi} + N$

With the wave functions for q^6-N and q^6-J/Ψ specified in the previous subsections, we can use the formula in Sec. III, with trivial changes in notations and spin quantum numbers, to calculate the total cross section of $\gamma + {}^3$He $\rightarrow [q^6]_{J/\psi} + N$. However, we need to multiply the results by the probability P_{q^6} of the N-$[q^6]$ component in ^{3}He; namely the results from using Eq. (19) is changed to

$$\frac{d\sigma}{d\Omega} \rightarrow P_{[q^6]} \times \left[\frac{d\sigma}{d\Omega} \right]_0, \quad (58)$$

where $[\frac{d\sigma}{d\Omega}]_0$ is calculated from using Eq. (19) and all subsequent equations in Sec. III A.

We first consider the case that $P_{[q^6]} = 0.7\%$ as determined in Refs. [18,19] from fitting the NN phase shifts up to 1 GeV. By using the parameters for models A_1 and A_2 listed in Table III, we obtain the results shown in Fig. 10. We observe that with the same small radius $\langle r^2 \rangle^{1/2} = 0.226$ fm for the produced $[q^6]_{J/\psi}$ system, the predicted cross sections are very close despite their potential range, measured by $1/\mu_{q^6}$, and coupling constant α_{q^6} can be very different. The same finding is also from comparing the predicted cross sections from the models B_1 and B_2, and also the models C_1 and C_2.

In the left-hand side of Fig. 11, we show the dependence of the predicted cross sections on P_{q^6} by comparing the cross sections from three models A_1, B_1, and C_1 listed in Table III.
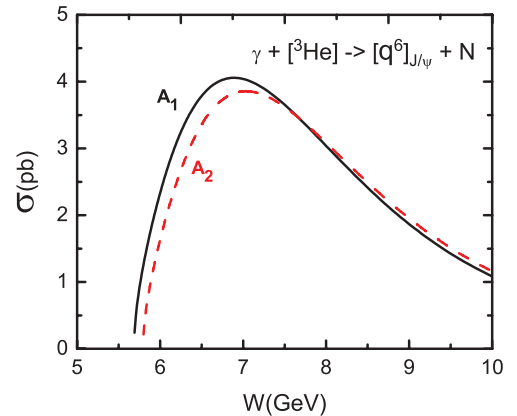

FIG. 10. (Color online) The total cross section of $\gamma + {}^3$He $\rightarrow [q^6]_{J/\psi} + N$ as function of the γ-^{3}He invariant mass W. The black solid and red dashed curves are for the case A_1 and A_2 in the Table III, respectively.
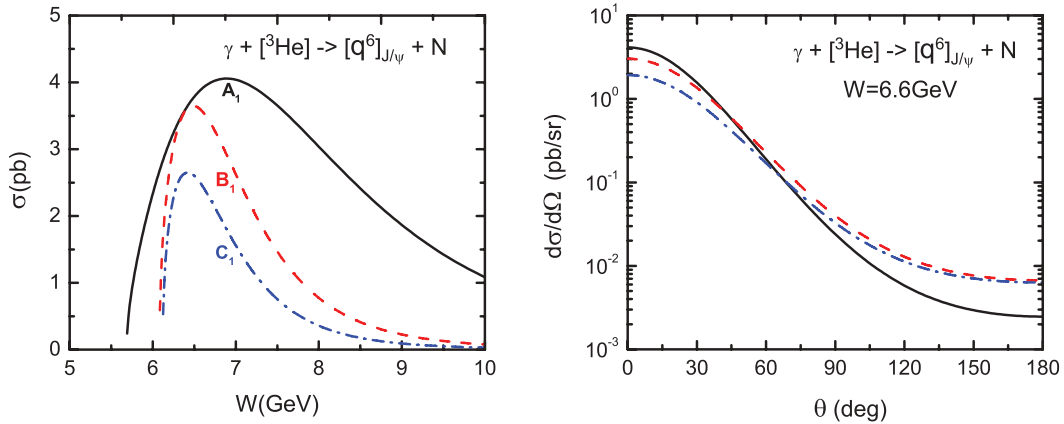
FIG. 11. (Color online) The black solid, red dashed, and blue dotted-dashed lines are from models A_1, B_1, and C_1 of Table III, respectively. Left: The total cross section of $\gamma + {}^3\text{He} \rightarrow [q^6]_{J/\psi} + N$ as function of the γ-${}^3\text{He}$ invariant mass W. Right: The differential cross section of $\gamma + {}^3\text{He} \rightarrow q^6_{[J/\psi]} + N$ of the outgoing N at γ-${}^3\text{He}$ invariant mass $W = 6.6$ GeV.

We observe that as P_{q^6} decreases, the peak is shifted to higher energies. Each case has different threshold energy due to their differences in binding energies, as seen in Table III. Their magnitudes are comparable despite their P_{q^6} are very different. We find that this is due to the fact that the cross section $[\frac{d\sigma}{d\Omega}]_0$ in Eq. (58) for the model with smaller $P_{q^6} = 0.7\%$ is a factor of about 10 larger than that for the model with larger $P_{q^6} = 6.38\%$, since this large momentum transfer reaction favors the production of $[q^6]_{J/\psi}$ with smaller size characterized by $\langle r^2 \rangle^{1/2}$ in Table III. The situation is similar to what we discussed in explaining the results shown in Fig. 4. Thus the magnitudes of the cross sections from three models at peak positions are comparable because the factor of about 10 difference in $[\frac{d\sigma}{d\Omega}]_0$ in Eq. (58) is compensated by the similar factor of about 10 in P_{q^6}. However, the three models have rather different energy dependence, as also seen in the left-hand side of Fig. 11. On the other hand, they are all forward peaked, as shown in the right-hand side of Fig. 11 for the differential cross sections at $W = 6.6$ GeV.

The results shown in Fig. 11 suggest that the upper bound of the predicted total cross sections of $\gamma + {}^3\text{He} \rightarrow [q^6]_{J/\psi} + N$ is about 2–4 pb.

V. SUMMARY AND DISCUSSIONS

We have presented predictions of the cross sections of $\gamma + {}^4\text{He} \rightarrow N + [{}^3\text{He}]_{J/\psi}$ reaction at energies near the J/Ψ production threshold. In the impulse approximation, the calculations have been performed by using several $\gamma + N \rightarrow J/\Psi + N$ models based on the Pomeron-exchange and pion-exchange mechanisms. The J/Ψ wave functions in $[{}^3\text{He}]_{J/\psi}$ are generated from various J/Ψ-nucleus potentials which are constructed by either using a procedure based on the Pomeron-quark coupling mechanism [7], or folding a J/Ψ-N potential $v_{J/\Psi,N}$ into the nuclear densities. We consider $v_{J/\Psi,N}$ derived from the effective field theory approach, lattice QCD, and Pomeron-quark coupling model. The upper bound of the predicted total cross sections is about 0.1–0.3 pb.

Clearly, our investigations are only for estimating the cross sections to facilitate the experimental considerations of

possible measurements of $[{}^3\text{He}]_{J/\Psi}$ bound states at Jefferson Laboratory. Several improvements are needed for more quantitative predictions. First we need precise data of $\gamma + p \rightarrow J/\Psi + p$ near threshold to distinguish several models we have considered and also to develop a more sophisticated model. We also need the data to pin down the J/Ψ-N interaction for a more realistic calculation of J/Ψ-nucleus potential such as the folding model considered in this work. One possibility is to use the $\pi + {}^2\text{H} \rightarrow p + J/\Psi + n$ reaction to extract the J/Ψ-N scattering length, as suggested in Ref. [4]. Alternatively, we can apply the model presented in this paper to determine the J/Ψ-N interactions by investigating the $\gamma + {}^2\text{H} \rightarrow p + J/\Psi + n$ reaction. Possible experiments on these two processes will be very useful. We of course also need to use more realistic wave functions for ${}^3\text{He}$ and ${}^4\text{He}$ while the s-wave oscillator wave functions employed in this investigation are reasonably consistent with the charge form factors calculated from the conventional nuclear models.

Motivated by the previous investigations [12,13] on the effects due to multiquark clusters in pp and $\gamma + {}^2\text{H} \rightarrow J/\Psi + n + p$, we have also considered the possibility of the production of a $[q^6] - J/\Psi$ bound state due to a six-quark $[q^6]$ cluster in ${}^3\text{He}$. The compound bag model of NN scattering and the quark cluster model of nuclei are used to estimate the $[q^6]$-N wave function in ${}^3\text{He}$ by imposing the condition that the sum of the contributions from $[q^6]$-N and NNN components to the ${}^3\text{He}$ charge form factor must be consistent with what are predicted by the conventional nuclear models [41] which explain the data very well. The upper bound of the predicted total cross sections of $\gamma + {}^3\text{He} \rightarrow [q^6]_{J/\Psi} + N$ is about 2–4 pb, depending on the model of $\gamma + N \rightarrow J/\Psi + N$ used in the calculations. If such bound states can be identified, it will open up a new window for investigating the role of the gluon field in determining the hadron structure.

[1] M. E. Peskin, Nucl. Phys. B **156**, 365 (1979).

[2] G. Bhanot and M. E. Peskin, Nucl. Phys. B **156**, 391 (1979).

[3] M. Luke, A. V. Manohar, and M. J. Savage, Phys. Lett. B **288**, 355 (1992).

[4] S. J. Brodsky and G. A. Miller, Phys. Lett. B **412**, 125 (1997).

[5] Taichi Kawanai and Shoichi Sasaki, Phys. Rev. D **82**, 091501 (2010).

[6] A. B. Kaidalov and P. E. Volkovitsky, Phys. Rev. Lett. **69**, 3155 (1992).

[7] S. J. Brodsky, I. A. Schmidt, and G. F. de Téramond, Phys. Rev. Lett. **64**, 1011 (1990).

[8] A. Donnachie and P. V. Landshoff, Nucl. Phys. B **244**, 322 (1984).

[9] Herman Feshbach, *Theoretical Nuclear Physics, Nuclear Reactions* (Wiley, New York, 1992).

[10] Z.-E. Meziani, K. Hafidi, X. Qian, N. Sparveris *et al.*, Proposal "Near Threshold Electroproduction of J/Ψ at 11 GeV", PR12-12-006 (2012), PAC39, Jefferson Laboratory (2012).

[11] Stanley J. Brodsky, SLAC-PUB-14985 (2012); SLAC-PUB-15050 (2012).

[12] S. J. Brodsky and G. F. de Teramond, Phys. Rev. Lett. **60**, 1924 (1988).

[13] S. J. Brodsky, E. Chudakov, P. Hoyer, and J. M. Laget, Phys. Lett. B **498**, 23 (2001).

[14] R. L. Jaffe and F. E. Low, Phys. Rev. D **19**, 2105 (1979); F. E. Low in *Pointlike Structure Inside and Outside Hadrons*, Proceedings of 1979 Erice Summer School, edited by A. Zichichi (Plenum, New York, 1979), p. 155.

[15] P. J. Mulders, Phys. Rev. D **26**, 3039 (1982); **28**, 443 (1983).

[16] Yu. A. Simonov, Phys. Lett. B **107**, 1 (1981); Nucl. Phys. A **416**, 109 (1984); Yad. Fiz. **38**, 1542 (1983) [Sov. J. Nucl. Phys. **38**, 939 (1983)].

[17] B. L. G. Bakker, I. L. Grach, and I. M. Narodetskii, Nucl. Phys. A **424**, 563 (1984).

[18] C. Fasano and T.-S. H. Lee, Phys. Rev. C **36**, 1906 (1987).

[19] C. Fasano and T.-S. H. Lee, Phys. Lett. B **217**, 9 (1989).

[20] H. J. Pirner and J. P. Vary, Phys. Rev. Lett. **46**, 1376 (1981).

[21] M. Namiki, K. Okano, and N. Oshimo, Phys. Rev. C **25**, 2157 (1982).

[22] P. V. Landshoff and O. Nachtmann, Z. Phys. C **35**, 405 (1987).

[23] J.-M. Laget and R. Mendez-Galain, Nucl. Phys. A **581**, 397 (1995).

[24] M. A. Pichowsky and T.-S. H. Lee, Phys. Rev. D **56**, 1644 (1997).

[25] A. I. Titov and T.-S. H. Lee, Phys. Rev. C **67**, 065205 (2003).

[26] Alvin Kiswandhi and Shin Nan Yang, Phys. Rev. C **86**, 015203 (2012); **86**, 019904(E) (2012).

[27] J. Beringer *et al.* (Particle Data Group), Phys. Rev. D **86**, 010001 (2012).

[28] Y. Oh and T.-S. H. Lee, Phys. Rev. C **66**, 045201 (2002).

[29] H. Gao, T.-S. H. Lee, and V. Marinov, Phys. Rev. C **63**, 022201(R) (2001).

[30] M. E. Binkley, C. Bohler, J. Butler, J. P. Cumalat, I. Gaines, M. Gormley, D. Harding, R. L. Loveless *et al.*, Phys. Rev. Lett. **48**, 73 (1982).

[31] B. H. Denby, V. K. Bharadwaj, D. J. Summers, A. M. Eisner, R. G. Kennett, A. Lu, R. J. Morrison, M. S. Witherell *et al.*, Phys. Rev. Lett. **52**, 795 (1984).

[32] R. Barate *et al.* (NA14 Collaboration), Z. Phys. C **33**, 505 (1987).

[33] P. L. Frabetti *et al.* (E687 Collaboration), Phys. Lett. B **316**, 197 (1993).

[34] U. Camerini, J. G. Learned, R. Prepost, C. M. Spencer, D. E. Wiser, W. Ash, R. L. Anderson, D. Ritson *et al.*, Phys. Rev. Lett. **35**, 483 (1975).

[35] B. Gittelman, K. M. Hanson, D. Larson, E. Loh, A. Silverman, and G. Theodosiou, Phys. Rev. Lett. **35**, 1616 (1975).

[36] R. L. Anderson, Excess Muons and New Results in Ψ Photoproduction. SLAC-PUB-1471 (unpublished).

[37] S. Aid *et al.* (H1 Collaboration), Nucl. Phys. B **472**, 3 (1996); A. Aktas *et al.* (H1 Collaboration), Eur. Phys. J. C **46**, 585 (2006).

[38] J. Breitweg *et al.* (ZEUS Collaboration), Z. Phys. C **76**, 599 (1997); S. Chekanov *et al.* (ZEUS Collaboration), Eur. Phys. J. C **24**, 345 (2002); Nucl. Phys. B **695**, 3 (2004); M. Derrick *et al.* (ZEUS Collaboration), Phys. Lett. B **350**, 120 (1995).

[39] R. Hofstadter, Annu. Nucl. Sci. **7**, 231 (1957); J. S. McCarthy *et al.*, Phys. Rev. C **15**, 1396 (1977).

[40] Aage Bohr and Ben R. Mottelson, *Nuclear Structure*, Vol. I (W. A. Benjamin, Inc., New York, 1969).

[41] J. Carlson and R. Schiavilla, Rev. Mod. Phys. **70**, 743 (1997); L. E. Marcucci, D. O. Riska, and R. Schiavilla, Phys. Rev. C **58**, 3069 (1998).

[42] T.-S. H. Lee and A. Matsuyama, Phys. Rev. C **32**, 516 (1985).

[43] H. Feshbach, A. Gal, and J. Hufner, Ann. Phys. (NY) **66**, 20 (1971).

[44] T.-S. H. Lee and S. Chakravarti, Phys. Rev. C **16**, 273 (1977).